



RESEARCH LETTER

10.1002/2015GL067353

Key Points:

- ACE-FTS first to observe N₂O production via energetic particle precipitation in lower thermosphere
- N₂O produced in mesosphere-lower thermosphere descends into upper stratosphere during polar winter
- N₂O is not a good dynamical tracer in polar winter upper stratosphere

Correspondence to:

K. A. Walker,
kwalker@atmosph.physics.utoronto.ca

Citation:

Sheese, P. E., K. A. Walker, C. D. Boone, P. F. Bernath, and B. Funke (2016), Nitrous oxide in the atmosphere: First measurements of a lower thermospheric source, *Geophys. Res. Lett.*, 43, 2866–2872, doi:10.1002/2015GL067353.

Received 8 DEC 2015

Accepted 23 FEB 2016

Accepted article online 27 FEB 2016

Published online 16 MAR 2016

Nitrous oxide in the atmosphere: First measurements of a lower thermospheric source

Patrick E. Sheese¹, Kaley A. Walker^{1,2}, Chris D. Boone², Peter F. Bernath³, and Bernd Funke⁴

¹University of Toronto, Toronto, Ontario, Canada, ²University of Waterloo, Waterloo, Ontario, Canada, ³Old Dominion University, Norfolk, Virginia, USA, ⁴Instituto de Astrofísica de Andalucía, Granada, Spain

Abstract Nitrous oxide (N₂O) is an important anthropogenic greenhouse gas, as well as one of the most significant anthropogenic ozone-depleting substances in the stratosphere. The satellite-based instrument Atmospheric Chemistry Experiment-Fourier Transform Spectrometer has been observing the Earth's limb since 2004 and derives profiles of N₂O volume mixing ratios in the upper troposphere to the lower thermosphere. The resulting climatology shows that N₂O is continuously produced in the lower thermosphere via energetic particle precipitation and enhanced N₂O is present at all latitudes, during all seasons. The results are consistent with an N₂O production source peaking near or above 94 km via low-energy particles, as well as a polar wintertime source near 70 km via medium energy particles. N₂O produced in the polar upper atmosphere descends each winter to as far down as ~40 km.

1. Introduction

Nitrous oxide (N₂O) is emitted into the atmosphere at the Earth's surface, through both natural (soil and ocean) and anthropogenic (agriculture) processes [e.g., Wayne, 2000; Brasseur and Solomon, 2005]. N₂O emitted at the surface is then transported into the stratosphere through the Brewer-Dobson circulation. Until recently, it was generally accepted that there are no atmospheric production sources of N₂O, and as such, the average concentration profile monotonically decreases with altitude. Model studies by Prasad and Zipf [2008] suggest that there is an N₂O production source in the atmosphere through the reaction of N₂ and electronically excited O₃ molecules, which is on the order of 7% of microbial and anthropogenic emissions. Prasad and Zipf [2008] also suggested that this production mechanism was on the order of 10–100 times greater than N₂O production through the three-body reaction between N₂, O(¹D), and an air molecule [Kajimoto and Cvetanovic, 1975]. Based on laboratory measurements in 1982 [Zipf and Prasad, 1982], it was proposed that there should be a lower thermospheric source of N₂O during times of strong geomagnetic activity, when energetic particle precipitation (EPP) would lead to enhancements of excited state N₂(A³Σ_u⁺) via electron impact,



Although, due to a complete lack of upper atmospheric N₂O measurements, this mechanism was largely dismissed as a potential atmospheric source of N₂O.

In January 2004, there was a sudden stratospheric warming (SSW) in the northern high latitudes that led to strong descent of upper atmospheric air, injecting NO_x (NO + NO₂) rich air into the upper stratosphere [e.g., Randall et al., 2009; Reddmann et al., 2010; Randall et al., 2015]. Semeniuk et al. [2008] reported that during this SSW, upper stratospheric observations from the satellite instrument ACE-FTS (Atmospheric Chemistry Experiment-Fourier Transform Spectrometer) exhibited anomalously high N₂O volume mixing ratios (VMRs), on the order of 2–6 ppbv, near 55 km. Using the Canadian Middle Atmosphere Model (CMAM), Semeniuk et al. [2008] were able to simulate the ACE-FTS version 2.2 (v2.2) N₂O VMRs (which were retrieved up to an altitude of only ~60 km). However, the CMAM simulations only introduced the reaction



into the model, where NO₂ and N(⁴S) were both produced by via medium energy EPP in the upper mesosphere, near ~75 km, and then transported down into the upper stratosphere. This is the mechanism that was concluded to be the source of upper stratospheric N₂O enhancements observed in MIPAS (Michelson Interferometer for Passive Atmospheric Sounding) data shortly after the October 2003 solar proton event [Funke et al., 2008a].

Funke et al. [2008b] reported that the MIPAS N₂O data set, which has an upper altitude limit of ~70 km, also exhibits stratospheric enhancements (N₂O concentrations of 0.5–6 ppbv near 60 km) during all observed polar winters between 2002 and 2004. The MIPAS data suggest that the predominant source of N₂O is near ~75 km via reaction (2) but that a significant amount (~20–40%) of enhanced N₂O could also have been produced near 95 km via reaction (1) [*Funke et al.*, 2008b]. Neither the MIPAS nor the ACE-FTS v2.2 N₂O observations extend into the lower thermosphere where these reactions are expected to occur. However, the most recent version, version 3.5 (v3.5), of the ACE-FTS data [*Boone et al.*, 2013] extends up to an altitude of 95 km.

2. Data Description

2.1. ACE-FTS on SCISAT

The ACE-FTS instrument [*Bernath et al.*, 2005] is a solar occultation limb sounder on the Canadian satellite SCISAT. It was launched in August of 2003 into a circular orbit near 650 km, at an inclination of 74°. The FTS is a high-resolution (0.02 cm⁻¹) spectrometer operating in the infrared between 750 and 4400 cm⁻¹ and observes the Earth's limb between altitudes of ~5–120 km with a vertical field of view of 3–4 km and a vertical sampling of 2–6 km. Since February 2004, ACE-FTS has regularly been providing volume mixing ratio (VMR) profiles of over 30 trace species and over 20 subsidiary isotopologues (of O₃, H₂O, CH₄, N₂O, OCS, CO, and CO₂), as well as profiles of temperature and pressure. The retrieval algorithm [*Boone et al.*, 2005; *Boone et al.*, 2013] is a nonlinear global least squares fitting technique that fits observed ACE-FTS infrared spectra to forward modeled spectra, based on absorption line strengths from HITRAN 2004 [*Rothman et al.*, 2005], with some updates. Temperature and pressure profiles are derived from CO₂ absorption measurements in multiple microwindows. This study uses v3.5 of the ACE-FTS level 2 data [*Boone et al.*, 2013], which has been interpolated onto a 1 km grid. In v3.5, N₂O profiles are retrieved between altitudes of 5 and 95 km, using 62 spectral microwindows ranging between 829 and 2241 cm⁻¹. The retrieval compensates for CHF₂Cl, CH₄, H₂O, O₃, CO, CO₂, HNO₃, and various isotopologues as interfering species. Version 2.2 of the ACE-FTS N₂O data was validated through comparisons with correlative data from airborne and satellite based instruments [*Strong et al.*, 2008]. Below 30 km, ACE-FTS is typically in reasonable agreement with coincident limb sounder data, to within 15–20%, and ACE-FTS typically exhibits a low bias on the order of 20–50% in the 30–50 km region [*Strong et al.*, 2008]. The mean difference between v2.2 and v3.5 N₂O VMR in this altitude region is less than ±0.5%. The ACE-FTS data set used in this study spans February 2004 to March 2013, and all data have been screened for outliers using version 1.1 of the ACE-FTS data quality flags, using the recommended screening methodology [*Sheese et al.*, 2015].

2.2. MEPED on NOAA 16 POES

Electron count rate measurements from the MEPED (Medium Energy Proton and Electron Detector) instrument [*Evans and Greer*, 2006] on the NOAA 16 POES SEM 2 (Polar-orbiting Operational Environmental Satellites Space Environment Monitor 2) satellite are used in this study. The 16 s average data were obtained from the National Geophysical Data Center website (<http://www.ngdc.noaa.gov/stp/satellite/poes/dataaccess.html>). Three MEPED channels for electron energies greater than 30 keV, greater than 100 keV, and greater than 300 keV (from here on referred to as M30, M100, and M300, respectively) are used (nominally low energy, medium energy, and high energy, respectively). Only data measured at latitudes greater than 60°N and geomagnetic latitudes greater than 55° (L shells greater than 3.0) are considered when comparing to ACE-FTS Arctic data. The MEPED data are converted to electron flux values and corrected for proton contamination, as described by *Yando et al.* [2011], and to avoid further contamination due to solar proton events (SPEs), data for days with SPEs (as listed by the NOAA Space Weather Prediction Center, <ftp://ftp.swpc.noaa.gov/pub/indices/SPE.txt>) have been omitted from the analysis. This has the strongest influence on the M100 and M300 data sets. Studies have also shown that not correcting for detector efficiencies leads to an inhomogeneity effect between SEM 1 and SEM 2 data, especially in the M30 data [e.g., *Asikainen and Mursula*, 2013; *Whittaker et al.*, 2014]. However, as only SEM 2 data are used in this study and only relative, not absolute, electron flux values are required for correlation calculations with ACE-FTS N₂O; the MEPED data have not been corrected for detector efficiencies.

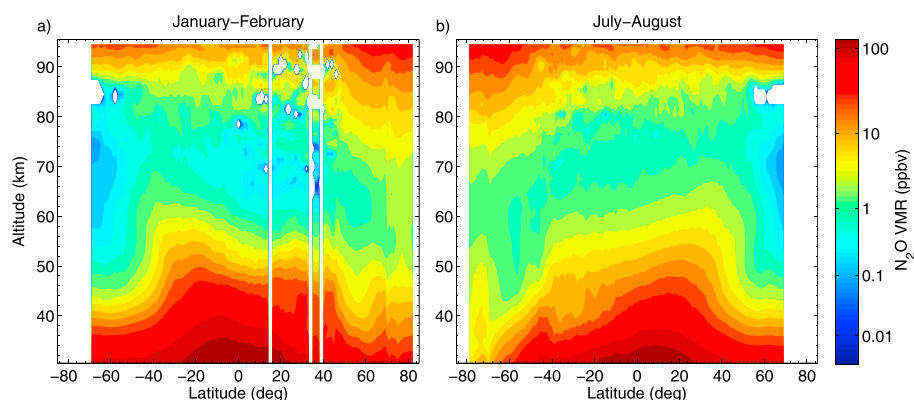


Figure 1. The 2004–2013 ACE-FTS N_2O VMR climatology for (a) January–February and (b) July–August. Values have been smoothed by the 5° running mean. Note that the color scale is logarithmic, white vertical bands represent latitudes that were not sampled, and white regions indicate negative mean values.

3. Results

In the following discussion, the terms Arctic and Antarctic are used to refer to latitude regions of $60\text{--}90^\circ\text{N}$ and $60\text{--}90^\circ\text{S}$, respectively, and the terms summer and winter are used to refer to either January–February or July–August, depending on the hemisphere.

A climatology of the 2004–2013 ACE-FTS v3.5 N_2O VMR profiles, extending from the stratosphere to the lower thermosphere has been produced, and Figures 1a and 1b show the N_2O climatology latitudinal cross sections for January–February and for July–August. The climatology was calculated at each altitude level by binning the data (both sunset and sunrise) into 1° bins and smoothing by the 5° mean. Hence, these are essentially zonal mean values. From Figure 1, it is clear that N_2O is being produced in the upper mesosphere-lower thermosphere in large quantities and is present at all latitudes. In the stratosphere, N_2O is distributed according to the Brewer-Dobson circulation, with strong stratospheric ascent in the summer lower latitudes, N_2O -depleted air in the summer polar regions, and descent at the winter pole throughout the upper stratosphere to lower thermosphere. However, there is a clear latitude-dependent N_2O source above 85 km that produces more N_2O nearer the poles than the tropics. For January–February at 94.5 km, the mean VMR within $\pm 30^\circ$ latitude is 12 ppbv and reaches 22 ppbv near the summer pole and 49 ppbv near the winter pole; for June–August, the mean VMR within $\pm 30^\circ$ is 16 ppbv and reaches 42 ppbv near the summer pole and 45 ppbv near the winter pole. This data set shows that in general, mesospheric N_2O VMRs are greater near the winter pole than the summer pole. This is likely due to increased sunlight in the summer high latitudes, increasing the likelihood of N_2O photolysis, especially at higher altitudes where there is greater actinic flux in the UV. As well, the mean circulation in the winter high latitudes transports N_2O produced in the lower thermosphere downward into the middle atmosphere. In the winter, both Arctic and Antarctic mean N_2O VMR profiles decrease with altitude to a minimum of ~ 0.9 ppbv near 59 km and then increase with altitude to ~ 40 ppbv near 94 km.

In the summer, both Arctic and Antarctic mean N_2O VMR profiles decrease with altitude to a local minimum of ~ 0.08 ppbv near 72 km, then exhibit a secondary peak near 80 km of ~ 0.25 ppbv and exhibit a pronounced minimum near 85 km where the mean retrieved values are negative (white regions in Figure 1), which are a consequence of the retrieval's tendency to overshoot to negative values in regions below a steep VMR gradient as a function of altitude. Values increase with altitude above the minimum and peak at an altitude above the ACE-FTS N_2O upper limit of 94.5 km. It is possible that the minimum near 85 km is in part due to the large increase in $\text{O}(^1\text{D})$, an N_2O sink ($\text{N}_2\text{O} + \text{O}(^1\text{D}) \rightarrow 2\text{NO}$). A major source of $\text{O}(^1\text{D})$ is through photolysis of O_3 in the Hartley band, and this region is immediately below the O_3 secondary peak, near 87 km. Since O_3 photolysis is at a minimum at the winter poles, similar minima are not expected nor seen in the polar winter mean profiles.

To get a sense of the altitude-dependent sources of N_2O in the polar upper atmosphere, the ACE-FTS data was compared to MEPED electron flux data—M30, M100, and M300. Daily values (smoothed by

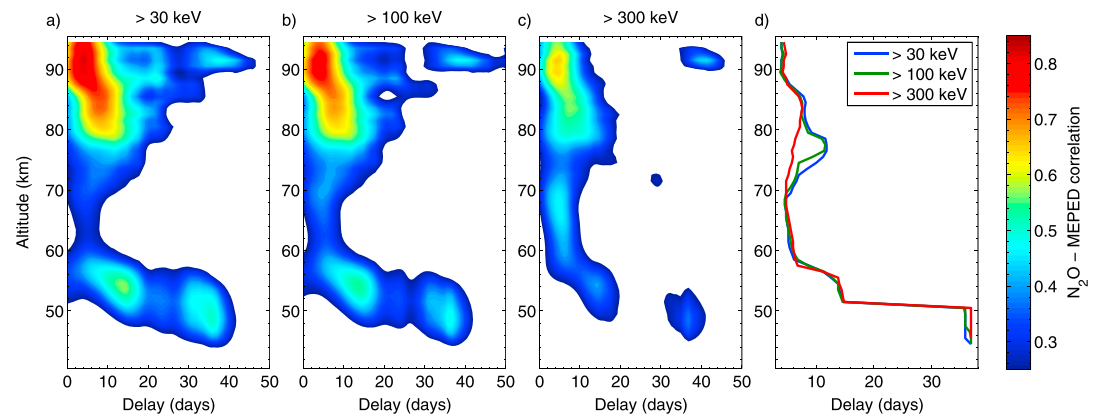


Figure 2. Correlation coefficient values for comparisons between Arctic winter N_2O data and time delayed (between 0 and 50 days) MEPED electron flux data in the (a) >30 keV, (b) >100 keV, and (c) >300 keV channels. (d) The delay time in all three channels that yields the greatest correlation with the ACE-FTS N_2O for all altitudes above 40 km. White regions indicate correlation coefficient values of 0.25 or less.

the 7 day means) of all three data sets were calculated by taking the mean of all values within ± 3.5 days and within $60\text{--}90^\circ\text{N}$. Values were only calculated for days that had at least one ACE-FTS measurement on that day. This was done at each altitude level for the N_2O data. All three weekly averaged MEPED time series were compared to similarly averaged ACE-FTS N_2O data at each altitude level above 40 km. At each altitude, correlation coefficients (Pearson's r) between the ACE-FTS and time delayed MEPED data were calculated, and Figures 2a–2d show the correlation coefficient profiles for delay values between 0 and 50 days.

Above 90 km, M30 shows the strongest correlation with ACE-FTS, with correlation coefficients near 0.8 with a MEPED time delay of approximately 4 days. If daily average values are used, instead of 7 day average values, the maximum correlation decreases slightly (due to the fact that winter N_2O has a long lifetime in this region and therefore can accumulate); however, the time delay value that yields the maximum correlation decreases to ~ 2 days at the highest altitude levels. This indicates that N_2O in this region is being predominantly produced in situ; however, N_2O is also produced at altitudes above the ACE-FTS detection limit and is being transported down into the region. With decreasing altitude the maximum M30 correlation decreases to 0.55 at 78 km, and the corresponding delay value increases approximately linearly from 4 days to 12 days. A linear fit to the M30 delay profile in this region yields a slope (a proxy N_2O descent rate) of 1.5 km/d. Similarly, the slope of the linear fit to the increase in delay time with decreasing altitude for the M100 correlations in this altitude region is 1.6 km/d. These are in reasonably good agreement with the mean downward descent rate determined from Whole Atmosphere Community Climate Model simulations of 1.1 km/d in the upper mesosphere [Smith *et al.*, 2011].

In the altitude region of 58–76 km, the strongest correlations with ACE-FTS N_2O are with the M300 time series, although the correlation is fairly weak, with correlation coefficients in the range of 0.45 to 0.5. A corresponding decrease in delay time (relative to delay times immediately above this region) is seen in this region. Even though electrons of >300 keV typically penetrate to ~ 60 km, a positive correlation with M300 near 90 km is expected, as these electrons will ionize N_2 at heights above where their ionization rate is at maximum. The fact that the observed M300 correlation is greater at 90 km than nearer 60 km is likely due to there being low to moderate correlation between the smoothed M300 and M30 data sets—increasing the correlation between M300 and the ACE-FTS N_2O data in the lower thermosphere.

Between 68 and 85 km, the delay time that yields the maximum correlation in the M300 data decreases with altitude and at 68 km M300 exhibits the strongest correlation of the three data sets, with a maximum correlation coefficient of 0.51 at a delay time of 5 days (using daily values, the delay time is approximately 3.5 days). These results would suggest that there is an in situ production mechanism in this region, which could be attributable to higher-energy precipitating particles. As discussed by Semeniuk *et al.* [2008] and Funke *et al.* [2008b], this production mechanism is likely N_2O produced via EPP-produced NO_2 and $N(^4S)$ (reaction (2)).

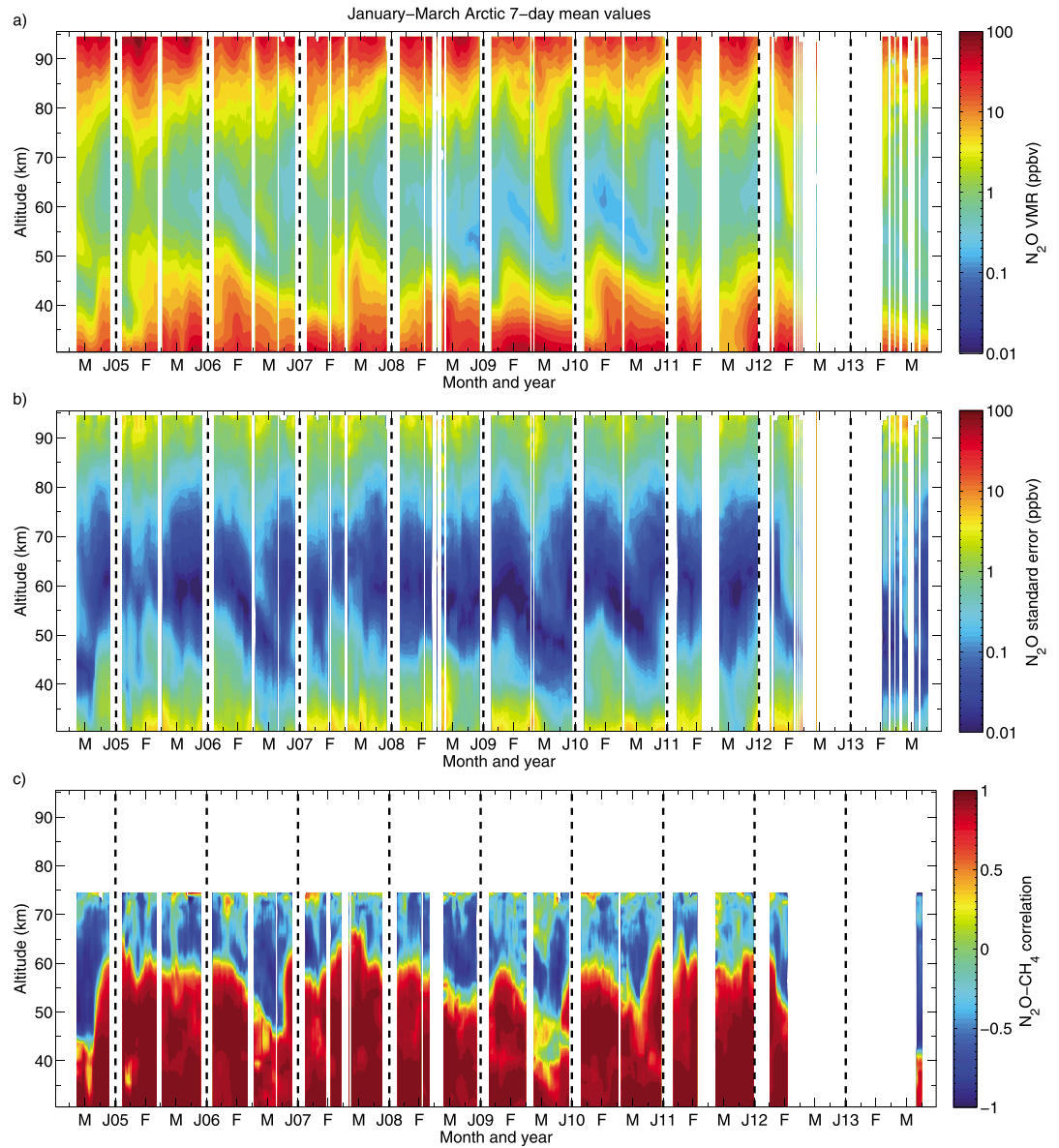


Figure 3. Arctic January–March ACE-FTS time series from 2004 to 2013. (a) N_2O VMR profiles (colors on logarithmic scale). White regions indicate days on which there were no Arctic ACE-FTS measurements that day or where the v3.5 data have not yet been processed, and the 1 day interval values represent the 7 day mean. (b) Corresponding N_2O standard error of the mean values. (c) Simultaneously measured N_2O - CH_4 correlation coefficients for all Arctic measurements within ± 3.5 days. Correlation profiles only extend to 75 km as this is the ACE-FTS CH_4 upper retrieval limit. White regions indicate days on which there were no Arctic ACE-FTS measurements, where the v3.5 data have not yet been processed or where there were less than 20 measurements within the ± 3.5 day period. Dashed lines indicate breaks in the time series.

Below 60 km, the delay times for the three MEPED data sets are all very similar. The delay time increases monotonically with decreasing altitude from ~ 6.5 days near 58 km to ~ 36 days near 48 km. In this altitude region, only moderate correlation is exhibited when comparing ACE-FTS with the M300 and M100 data sets, and the greatest correlation coefficients, in the range of 0.50–0.57, are exhibited when comparing with the M30 data set. The significant correlation coefficients (>0.5) for the M30 and M100 data down to ~ 45 km suggest that N_2O produced at altitudes above ~ 80 km [e.g., Fang *et al.*, 2010] descended to 45 km. Since no correlation coefficients greater than 0.25 were observed at any delay time below 44.5 km, the results suggest that the EPP-produced N_2O either did not descend to lower altitudes or represented too small a contribution to be distinguished from the background N_2O . These production sources need to be incorporated

into high-altitude global circulation models (GCMs) in order to fully capture the descent of N_2O and NO_x into the winter polar regions.

The ACE-FTS Arctic N_2O time series for January–March 2004–2013 is shown in Figure 3a with corresponding N_2O standard error of the mean values shown in Figure 3b. Intrusions, or “tongues,” of N_2O can be seen extending down into the stratopause region, especially in 2004, 2006, 2009, 2012, and 2013, where there were strong SSW events. In these years, these tongues of N_2O typically descend to minimum altitudes in the range of 45–55 km, with concentrations on the order of 1–3 ppbv. The strongest N_2O descent was in 2004, bringing concentrations of ~ 3 ppbv down to near 50 km and ~ 1.5 ppbv near 46 km (although there is currently a data gap in the v3.5 Arctic winter 2012 data, it is unlikely that the amount of N_2O descending in 2012 would have matched or exceeded that in 2004, due to the low level off EPP during that period). In January 2005, in the 60–70 km region, there is also an enhancement of N_2O VMR on the order of 2–3 ppbv, which follows the SPE that began on 15 January 2005.

If all the N_2O brought down to 50 km during or following a SSW (~ 2 ppbv) was then converted to NO_x , this would account for roughly 5–25% of the NO_x in the region. Since estimates of the percentage of upper stratospheric ozone destroyed by EPP-produced NO_x are approximately 5–9% [Reddmann *et al.*, 2010; Funke *et al.*, 2005], the effect of EPP-produced N_2O on upper stratospheric ozone would be a maximum of $\sim 2\%$ of the total destruction. However, this ignores the effect of N_2O being converted to NO_x prior to reaching the upper stratosphere-lower mesosphere (USLM), during the descent of the air mass. A comprehensive GCM study would be needed to determine the total contribution of EPP-produced N_2O on stratospheric ozone loss.

Under the assumption that the only atmospheric N_2O sources are surface emissions, one would expect simultaneous measurements of N_2O and CH_4 to be very strongly correlated throughout the stratosphere and into the mesosphere until the chemical lifetimes of one or both of the species becomes much shorter than local transport timescales. At each altitude level, correlation coefficient values for all simultaneously measured N_2O and CH_4 VMR values within ± 3.5 days, and within 60–90°N were calculated and are shown in Figure 3c. Data are only shown for days that have at least 20 simultaneous N_2O and CH_4 measurements within the 7 day time span, and data are not shown for days on which there are no measurements taken on that day. As seen in Figure 3c, simultaneous ACE-FTS N_2O and CH_4 measurements are typically very strongly correlated in the lower and middle stratosphere, with an average correlation coefficient greater than 0.9. However, N_2O and CH_4 are not significantly correlated at altitudes as low as 40 km, where there is a mix of both tropospheric and upper atmospheric N_2O due to downward descent. N_2O is often used as a stratospheric dynamical tracer, although typically at altitudes below 30–35 km [e.g., Jost *et al.*, 2002; El Amraoui *et al.*, 2008; Nedoluha *et al.*, 2015]. However, some studies make use of N_2O as a dynamical tracer at higher altitudes [e.g., Nielsen *et al.*, 1994; Khosrawi *et al.*, 2004; Ricaud *et al.*, 2005] and can infer that high N_2O VMR values in the upper stratosphere indicate upward transport of N_2O -rich air. Therefore, it may be ill advised to use N_2O as a dynamical tracer in the polar upper stratosphere.

4. Summary

From ACE-FTS measurements, it has been shown that N_2O is being produced in the lower thermosphere, and polar winter concentrations are typically on the order of 20–40 ppbv in the 90–95 km region. The production source is ultimately EPP via reaction (1) in the lower thermosphere and reaction (2) in the middle mesosphere to upper mesosphere.

As N_2O is potentially the most important ozone-depleting substance currently being emitted into the atmosphere [Ravishankara *et al.*, 2009], understanding the effect of geomagnetic activity on N_2O production and understanding the balance between surface and EPP-produced N_2O in the upper stratosphere-lower mesosphere (USLM) may be required for projecting future ozone levels in the upper stratosphere. These production sources need to be incorporated into high-altitude global circulation models in order to fully capture the descent of N_2O and NO_x into the winter polar regions and to quantify their effects on upper stratospheric ozone depletion.

In the Arctic winter, when there is downward descent, N_2O that originated in the mesosphere-lower thermosphere is transported into the lower mesosphere. When there are SSW events, upper atmospheric

N₂O can be transported down into the upper stratosphere, to altitudes as low as ~45 km. As such, in this region, N₂O and CH₄ are often anticorrelated or uncorrelated at altitudes as low as 40 km, where the two are expected to be highly correlated. Therefore, future studies should use caution when using N₂O as a dynamical tracer in this region.

Acknowledgments

This project was funded by the Canadian Space Agency (CSA). The Atmospheric Chemistry Experiment is a Canadian-led mission mainly supported by the CSA. The authors wish to thank the three anonymous reviewers for their time and valuable contributions. The ACE-FTS Level 2 N₂O data used in this study can be obtained upon request from the corresponding author (kwalker@atmosph.physics.utoronto.ca) or via the ACE-FTS website (registration required), <http://www.ace.uwaterloo.ca>. The MEPED data used in this study are freely available via <https://ngdc.noaa.gov/stp/satellite/poes/dataaccess.html>.

References

- Asikainen, T., and K. Mursula (2013), Correcting the NOAA/MEPED energetic electron fluxes for detector efficiency and proton contamination, *J. Geophys. Res. Space Physics*, *118*, 6500–6510, doi:10.1002/jgra.50584.
- Bernath, P. F., et al. (2005), Atmospheric Chemistry Experiment (ACE): Mission overview, *Geophys. Res. Lett.*, *32*, L15501, doi:10.1029/2005GL022386.
- Boone, C. D., R. Nassar, K. A. Walker, Y. Rochon, S. D. McLeod, C. P. Rinsland, and P. F. Bernath (2005), Retrievals for the Atmospheric Chemistry Experiment Fourier-Transform Spectrometer, *Appl. Opt.*, *44*, 7218–7231, doi:10.1364/AO.44.007218.
- Boone, C. D., K. A. Walker, and P. F. Bernath (2013), *Version 3 Retrievals for the Atmospheric Chemistry Experiment Fourier Transform Spectrometer (ACE-FTS), The Atmospheric Chemistry Experiment ACE at 10: A Solar Occultation Anthology*, pp. 103–127, A. Deepak Publishing, Hampton, Va.
- Brasseur, G. P., and S. Solomon (2005), *Aeronomy of the Middle Atmosphere*, 3rd ed., Springer, Dordrecht.
- El Amraoui, L., V.-H. Peuch, P. Ricaud, S. Massart, N. Semane, H. Teyssèdre, D. Cariolle, and F. Karcher (2008), Ozone loss in the 2002–2003 Arctic vortex deduced from the assimilation of Odin/SMR O₃ and N₂O measurements: N₂O as a dynamical tracer, *Q. J. R. Meteorol. Soc.*, *134*, 217–228, doi:10.1002/qj.191.
- Evans, D. S., and M. S. Greer (2006), Polar orbiting satellite space environment monitor-2: Instrument descriptions and archive data documentation, *NOAA Tech. Memo.*, NOAA, Washington, D. C.
- Fang, X., C. E. Randall, D. Lummerzheim, W. Wang, G. Lu, S. C. Solomon, and R. A. Frahm (2010), Parameterization of monoenergetic electron impact ionization, *Geophys. Res. Lett.*, *37*, L22106, doi:10.1029/2010GL045406.
- Funke, B., M. López-Puertas, S. Gil-López, T. von Clarmann, G. P. Stiller, H. Fischer, and S. Kellmann (2005), Downward transport of upper atmospheric NO_x into the polar stratosphere and lower mesosphere during the Antarctic 2003 and Arctic 2002/2003 winters, *J. Geophys. Res.*, *110*, D24308, doi:10.1029/2005JD006463.
- Funke, B., M. García-Comas, M. López-Puertas, N. Glatthor, G. P. Stiller, T. von Clarmann, K. Semeniuk, and J. C. McConnell (2008a), Enhancement of N₂O during the October–November 2003 solar proton events, *Atmos. Chem. Phys.*, *8*, 3805–3815, doi:10.5194/acp-8-3805-2008.
- Funke, B., M. López-Puertas, M. García-Comas, G. P. Stiller, T. von Clarmann, and N. Glatthor (2008b), Mesospheric N₂O enhancements as observed by MIPAS on Envisat during the polar winters in 2002–2004, *Atmos. Chem. Phys.*, *8*, 5787–5800, doi:10.5194/acp-8-5787-2008.
- Jost, H., et al. (2002), Mixing events revealed by anomalous tracer relationships in the Arctic vortex during winter 1999/2000, *J. Geophys. Res.*, *107*(D24), 4795, doi:10.1029/2002JD002380.
- Kajimoto, O., and R. J. Cvetanovic (1975), Formation of nitrous oxide in reactions of O(¹D₂) atom with nitrogen, *J. Chem. Phys.*, *64*, 1005–1015, doi:10.1063/1.432308.
- Khosrawi, F., R. Müller, M. H. Proffitt, and H. Nakajima (2004), Monthly averaged ozone and nitrous oxide from the Improved Limb Atmospheric Spectrometer (ILAS) in the Northern and Southern Hemisphere polar regions, *J. Geophys. Res.*, *109*, D10301, doi:10.1029/2003JD004365.
- Nedoluha, G. E., I. S. Boyd, A. Parrish, R. M. Gomez, D. R. Allen, L. Froidevaux, B. J. Connor, and R. R. Querel (2015), Unusual stratospheric ozone anomalies observed in 22 years of measurements from Lauder, New Zealand, *Atmos. Chem. Phys.*, *15*, 6817–6826, doi:10.5194/acp-15-6817-2015.
- Nielsen, J. E., R. B. Rood, A. R. Douglass, M. C. Cerniglia, D. J. Allen, and J. E. Rosenfield (1994), Tracer evolution in winds generated by a global spectral mechanistic model, *J. Geophys. Res.*, *99*, 5399–5420, doi:10.1029/93JD03578.
- Prasad, S. S., and E. C. Zipf (2008), Atmospheric production of nitrous oxide from excited ozone and its potentially important implications for global change studies, *J. Geophys. Res.*, *113*, D15307, doi:10.1029/2007JD009447.
- Randall, C. E., V. L. Harvey, D. E. Siskind, J. France, P. F. Bernath, C. D. Boone, and K. A. Walker (2009), NO_x descent in the Arctic middle atmosphere in early 2009, *Geophys. Res. Lett.*, *36*, L18811, doi:10.1029/2009GL039706.
- Randall, C. E., V. L. Harvey, L. A. Holt, D. R. Marsh, D. Kinnison, B. Funke, and P. F. Bernath (2015), Simulation of energetic particle precipitation effects during the 2003–2004 Arctic winter, *J. Geophys. Res. Space Physics*, *120*, 5035–5048, doi:10.1002/2015JA021196.
- Ravishankara, A. R., J. S. Daniel, and R. W. Portmann (2009), Nitrous oxide (N₂O): The dominant ozone-depleting substance emitted in the 21st century, *Science*, *326*, 123–125, doi:10.1126/science.1176985.
- Reddmann, T., R. Ruhnke, S. Versick, and W. Kouker (2010), Modeling disturbed stratospheric chemistry during solar-induced NO_x enhancements observed with MIPAS/ENVISAT, *J. Geophys. Res.*, *115*, D00111, doi:10.1029/2009JD012569.
- Ricaud, P., et al. (2005), Polar vortex evolution during the 2002 Antarctic major warming as observed by the Odin satellite, *J. Geophys. Res.*, *110*, D05302, doi:10.1029/2004JD005018.
- Rothman, L. S., et al. (2005), The HITRAN 2004 molecular spectroscopic database, *J. Quant. Spectrosc. Radiat. Transfer*, *96*, 139–204, doi:10.1016/j.jqsrt.2004.10.008.
- Semeniuk, K., J. C. McConnell, J. J. Jin, J. R. Jarosz, C. D. Boone, and P. F. Bernath (2008), N₂O production by high energy auroral electron precipitation, *J. Geophys. Res.*, *113*, D16302, doi:10.1029/2007JD009690.
- Sheese, P. E., C. Boone, and K. A. Walker (2015), Detecting physically unrealistic outliers in ACE-FTS atmospheric measurements, *Atmos. Meas. Tech.*, *8*, 741–750, doi:10.5194/amt-8-741-2015.
- Smith, A. K., R. R. Garcia, D. R. Marsh, and J. H. Richter (2011), WACCM simulations of the mean circulation and trace species transport in the winter mesosphere, *J. Geophys. Res.*, *116*, D20115, doi:10.1029/2011JD016083.
- Strong, K., et al. (2008), Validation of ACE-FTS N₂O measurements, *Atmos. Chem. Phys.*, *8*, 4759–4786, doi:10.5194/acp-8-4759-2008.
- Wayne, R. P. (2000), *Chemistry of Atmosphere*, 3rd ed., Oxford Univ. Press, Oxford.
- Whittaker, I. C., C. J. Rodger, M. A. Clilverd, and J.-A. Sauvaud (2014), The effects and correction of the geometric factor for the POES/MEPED electron flux instrument using a multisatellite comparison, *J. Geophys. Res. Space Physics*, *119*, 6386–6404, doi:10.1002/2014JA020021.
- Yando, K., R. M. Millan, J. C. Green, and D. S. Evans (2011), A Monte Carlo simulation of the NOAA POES medium energy proton and electron detector instrument, *J. Geophys. Res.*, *116*, A10231, doi:10.1029/2011JA016671.
- Zipf, E. C., and S. S. Prasad (1982), A mesospheric source of nitrous oxide, *Nature*, *295*, 133–135, doi:10.1038/295133a0.